Journal of Intelligent and Robotic Systems **20:** 375–402, 1997.

Robust Sliding-mode Control of Nine-link Biped Robot Walking

SPYROS G. TZAFESTAS and THANASSIS E. KRIKOCHORITIS
Intelligent Robotics and Automation Laboratory, Department of Electrical and Computer Engineering, National Technical University of Athens, 15773, Zografou Campus, Athens, Greece

COSTAS S. TZAFESTAS
Laboratoire Robotique de Paris-CRIIF, Univ. P. et M. Curie, 10-12 av. de l'Europe 78140 Velizy-Villacoublay, France

(Received: 18 December 1996; accepted: 16 June 1997)

Abstract. A nine-link planar biped robot model is considered which, in addition to the main links (i.e., legs, thighs and trunk), includes a two-segment foot. First, a continuous walking pattern of the biped on a flat terrain is synthesized, and the corresponding desired trajectories of the robot joints are calculated. Next, the kinematic and dynamic equations that describe its locomotion during the various walking phases are briefly presented. Finally, a nonlinear robust control approach is followed, motivated by the fact that the control which has to guarantee the stability of the biped robot must take into account its exact nonlinear dynamics. However, an accurate model of the biped robot is not available in practice, due to the existence of uncertainties of various kinds such as unmodeled dynamics and parameter inaccuracies. Therefore, under the assumption that the estimation error on the unknown (probably time-varying) parameters is bounded by a given function, a sliding-mode controller is applied, which provides a successful way to preserve stability and achieve good performance, despite the presence of strong modeling imprecisions or uncertainties. The paper includes a set of representative simulation results that demonstrate the very good behavior of the sliding-mode robust biped controller.

Key words: nine-link biped robot, biped locomotion, biped walking pattern, biped kinematic model, biped dynamic model, sliding-mode control.

1. Introduction

The study of the motion of living organisms by means of legs, especially the locomotion of bipeds, has always been a challenging problem to scientists of different vocations: biologists, physiologists, medicine specialists, mathematicians, and engineers. In spite of their efforts, however, this problem has not yet been solved in a satisfactory way.

One of the primary motivations for designing biped robots is to perform tasks in environments that are too dangerous for human beings. To be a satisfactory substitute for the human being, the robot must be able to enter a region originally designed for human access, and perfom tasks that are not already automated and normally require the capabilities of a person. One measure of the success of a biped design is how well it can emulate the agility of a human being. Therefore, a

useful biped robot needs feet. It is not possible for a passive platform to stand in a single, stable position if it is supported on only two points. However, a dynamic system can balance on two points like stilts, if the supporting points are allowed to move and are controlled by a sufficiently sophisticated control system. The stiff legged stilt biped must remain in a continuous state of motion to maintain balance.

In this paper a 9-link planar biped model is studied which includes not only the main links: legs, thighs, and trunk, but also a two segments foot. This biped has two hip, two knee, two ankle, and two metatarsal joints, with one d.o.f. each of them. The motion is constrained on the sagittal plane, and as a consequence, the total number of degrees of freedom is going to be limited enough, always depending on the phase of the walking being executed. This two dimensional motion can in fact be achieved in reality, as it was shown by the Kenkyaku-2 biped [1] which has a steel pipe attached to the lowest end of the leg in order to maintain the lateral balance. The goal for the choice of this model is the achievement of a more satisfactory substitute for the anthropomorphic gait, giving special attention to the model of the foot. Most of the previous biped studies consider the foot as one solid element. Here, each foot is composed of two rigid parts connected at the transverse tarsal joint. The calcancus and talus, as a single unit, form the proximal segment, and the remaining bones and joints of the foot the distal segment. The work presented here is a continuation of that described in [2], where a 5-link biped robot was considered (i.e., the robot without the two-segment feet).

The structure of the paper is as follows: Section 2 describes the synthesis of a continuous walking pattern consisting of several phases (single-leg-supporting phase with non-kick or kick-action, leg support-exchange, collision of the swing leg with the ground), and derives the corresponding trajectories of the robot joints. Section 3 provides the kinematic and Lagrange dynamic models of the 9-link biped, which can be derived as in [2], and are fully reported in [5]. Section 4, which represents the main body of the paper, presents the detailed derivation of the sliding-mode controller as applied to the present 9-link biped robot, including a discussion of the general hierarchical structure of robot control systems. Finally, Section 5 gives a set of simulation experimental results which show the effectiveness of the controller.

2. The Walking Pattern

Among the analytical models of walking the most popular one is based on the hypothesis that walking is performed such that to have the least expenditure of energy. Indeed, experimental findings suggest that human walking is a learned activity which aims to keep energy consumption as low as possible [3].

In our 9-link biped robot model, it is assumed that at the middle of the supporting leg period, i.e., when the swing leg moves before the suporting leg, a new phase of the gait exists. This is the *kick phase*, where an ankle motion

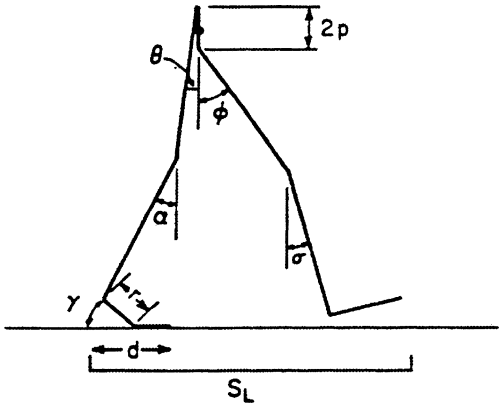

Figure 1. A ballistic walking model.

of the supporting leg is achieved, so that a maximum of the vertical force just before the collision appears. Furthemore, it is assumed that the torque, applied to the knee joint is zero, the desired trajectories of the angles θ and γ are specified as a function of α, and in addition the reference signals are chosen so as to use the effects of the gravity in a way that increases the angular momentum during the single leg supporting phase (see Figure 1).

Therefore, trying to utilize the gravity effect skillfully, the following walking pattern is adopted:

(1) The body is always kept upright.
(2) The knee of the supporting leg extends straight, and, as a result, the first assumption is satisfied, since the relation between the thigh angle θ and the shank angle α is $\theta = \alpha$.
(3) The ankle and foot joint of the supporting leg is free except for the kick-phase.
(4) The foot of the swing leg is kept parallel to the ground.
(5) The leg-support-exchange is done in an instant. This means that the biped locomotion has no double-leg-supporting phase, and therefore immediately after the touchdown of the swing leg, the exchange of the supporting leg takes place.
(6) At the touchdown, the knee joint of the swing leg is kept in bending state.
(7) The touchdown of the swing leg is assumed to occur in two stages. Firstly, the toes of the swing leg take a collision with the ground, and then the collision of the heel follows.
(8) The same reference signals are supplied at each step repeatedly.

Condition (6) has two effects, namely a decrease of the loss of the angular momentum at the leg-support-exchange phase, and an increase of the angular momentum during the single-leg-supporting phase. Condition (3) has the following three effects:

(i) A reduction of the up and down movement of the body.

(ii) A decrease of the loss of angular momentum at leg-support-exchange (due to kick-action).

(iii) An additional decrease of the loss of angular momentum in leg-support-exchange (due to the fact that the robot rotates around the ankle joint of the supporting leg in non-kick-phase, and around the tiptoe of the same leg in kick-phase), and an increase of the duration in which the clockwise torque due to gravity acts on the robot system (due to kick-action) [1].

According to condition (2): (i) the ankle angle is selected to be always constant at 90° ($qr_2(t) = 1.57$ rads), and (ii) the reference signal $qr_3(t)$ of the knee joint of the supporting leg is kept to be always zero. Similarly, according to condition (4), the reference signal $qr_8(t)$ which reprsents the motion of the foot joint is kept always constant at 110° ($qr_8(t) = 1.92$ rads), while at the same time the reference signal $qr_7(t)$ of the swing leg ankle joint will have to be kept constant at 90° ($qr_7(t) = 1.57$ rads), when the swing leg is before the supporting leg.

The reference signals $qr_5(t)$ and $qr_6(t)$ play the most important role for the synthesis of our 9-link biped robot gait. Before the collision of the swing leg, these signals must take constant values qrs_5 and qrs_6, respectively, in order for the position of the robot at the moment of collision to be the same in every step, without taking into account the small deviations of each gait time. In addition to the above condition, condition (6) must be satisfied, i.e., the knee joint of the swing leg must be kept in bending state. This way, if the values $qrs_5 = 0.471$ rads $= 27°$ and $qrs_6 = 0.471$ rads $= 27°$ are assumed, after a short period the shin of the swing leg is indeed kept vertical. Also, in analogy with the reference signal $qr_7(t)$, for the short period during which the swing leg is behind the supporting leg, the signal $qr_6(t)$ is desired to take values larger than 27°.

According to condition (3), the torque at the foot joint of the supporting leg is applied only during the kick phase. Therefore, the signal $qr_1(t)$ will be kept at the constant value of 110° ($qr_1(t) = 1.92$ rads) during the first phase, and then during the kick phase it will be extended up to about 130°, an angle which is large enough for the collision to be achieved. Finally, the angular momentum might become larger due to the effect of the torque caused by the gravity. Therefore, it is necessary for the swing leg (i.e., for the angular position $qr_5(t)$) to move forward quickly so that the period, during which the c.o.g. of the robot is before the ankle joint of the supporting leg, is larger than the period when the c.o.g. is behind the ankle joint.

The reference signals shown in Figure 2 describe the change of the angular position of the robot joints during the first two steps (1st step $0 \rightarrow 1.3$ s, 2nd step $1.3 \rightarrow 3.3$ s). Note that the reference signals during the first step are a little different, since the robot starts walking from the upright posture. The signals of the second step are recurrently used at every other step.

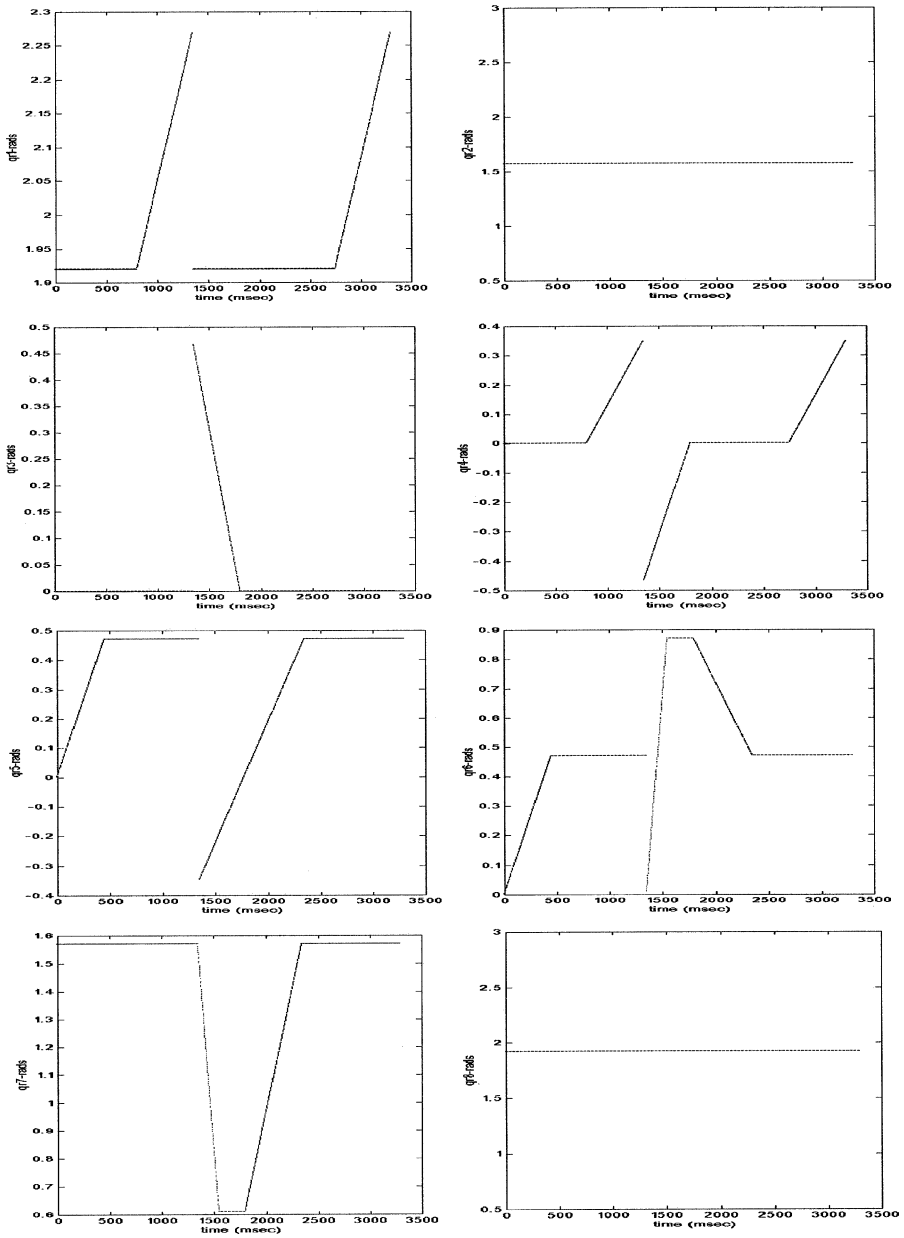

Figure 2. Reference signals for steady walking on an horizontal plane surface.

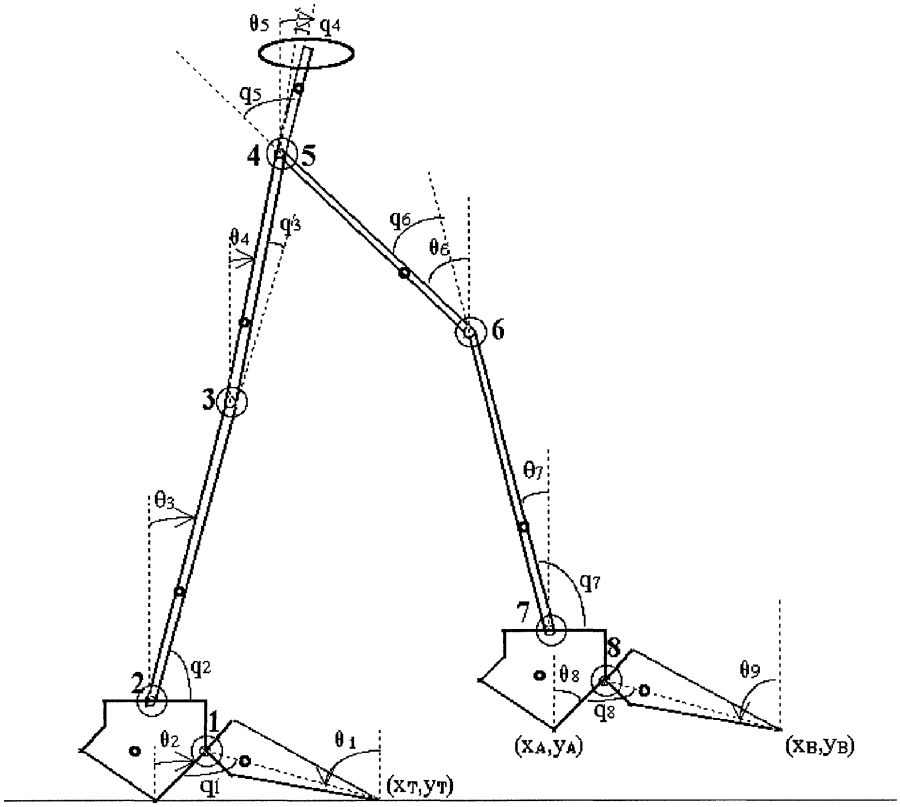

Figure 3. 9-link planar biped robot model.

3. Kinematic and Dynamic Model of the 9-link Biped Robot

The methodology that has been applied to find the kinematic and dynamic models of the 9-link biped robot is similar to the one that has been used for the 5-link biped robot in [2].

3.1. KINEMATIC MODEL

The 9-link biped under consideration is shown in Figure 3. It includes the *trunk* (link 5) and four links in each leg which represent the *thigh* (links 4 and 6), the *shin* (links 3 and 7), the *heel* (links 2 and 8) and the *metatarsal* (links 1 and 9). The links labeled l_i ($i = 1, \ldots, 9$) are joined together at ideal pin joints. Hence, it has two hip joints (joints 4 and 5), two knee joints (joints 3 and 6), two ankle joints (joints 2 and 7) and two metatarsal joints (joints 1 and 8), which are assumed to be ideal (without friction) rotational joints (with one d.o.f. each of them) driven by independent electric DC motors. At each joint, except the one which contacts the ground, there is an ideal torque τ_i. Since the biped motion

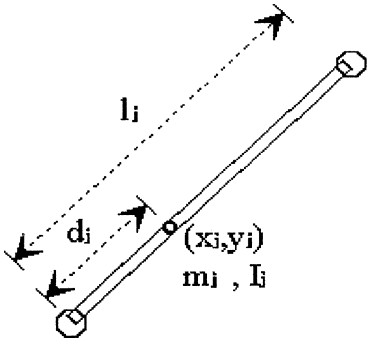

Figure 4. Parameters of the ith link.

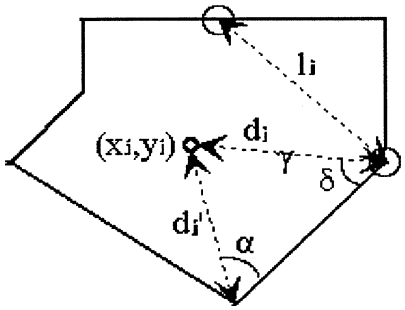

Figure 5. Parameters of the heel.

Table I. Nine-link biped model paramaters (heel angles (rads): $\alpha = 0.523$, $\varepsilon = 2.4436$, $\gamma = 1.396$, $\delta = 0.872$)

Link	Inertia I_i (kg/m)	Mass m_i (kg)	Radius d_i (m)	Length L_i (m)
1	1/6000	0.6	0.0828	0.1077
			0.05 (d_2)	
2	1/6000	0.6		0.05
			0.056 (d_2)	
3	0.105	4.550	0.267	0.502
4	0.089	7.630	0.247	0.431
5	2.350	49	0.280	0.827
6	0.089	7.630	0.247	0.431
7	0.105	4.550	0.267	0.502
			0.05 (d_8)	
8	1/6000	0.6		0.05
			0.056 (d_8)	
9	1/6000	0.6	0.0828	0.1077

is constrained to be on the sagittal plane, for a definite description, we use as generalized variables the set of the angles of each link i with the vertical, which are denoted as θ_i. The direction of the θ_i is as shown in Figure 3.

Each link has four parameters, namely the link mass m_i, its moment of inertia about the c.o.g. I_i, the length of the link l_i, and the distance between the c.o.g. and the lower joint d_i. Figure 4 shows these parameters for the ith link. For the heel, the notation is somewhat different (Figure 5). The numerical values of these parameters were drawn from [4] and are listed in Table I.

The kinematic model which describes the relation between the velocity of the foot of the swing leg and the change of generalized variables, is described by the following equations (the details are given in [5]):

$$\begin{aligned}
\mathbf{V}_A = \begin{bmatrix} \dot{x}_A \\ \dot{y}_A \end{bmatrix} &= \begin{bmatrix} -l_1 \cos\theta_1 \\ -l_1 \sin\theta_1 \end{bmatrix} \dot{\theta}_1 + \begin{bmatrix} -l_2 \cos(\theta_2 + \gamma) \\ l_2 \sin(\theta_2 + \gamma) \end{bmatrix} \dot{\theta}_2 \\
&+ \begin{bmatrix} l_3 \cos\theta_3 \\ -l_3 \sin\theta_3 \end{bmatrix} \dot{\theta}_3 + \begin{bmatrix} l_4 \cos\theta_4 \\ -l_4 \sin\theta_4 \end{bmatrix} \dot{\theta}_4 \\
&+ \begin{bmatrix} l_6 \cos\theta_6 \\ l_6 \sin\theta_6 \end{bmatrix} \dot{\theta}_6 + \begin{bmatrix} l_7 \cos\theta_7 \\ l_7 \sin\theta_7 \end{bmatrix} \dot{\theta}_7 \qquad (1) \\
&+ \begin{bmatrix} l_8 \cos(\theta_8 + \gamma) - d_8 \cos(\theta_8 + \delta) - d'_8 \cos(\theta_8 - \alpha) \\ -l_8 \sin(\theta_8 + \gamma) - d_8 \sin(\theta_8 + \delta) - d'_8 \sin(\theta_8 - \alpha) \end{bmatrix} \dot{\theta}_8 \\
\mathbf{V}_B = \begin{bmatrix} \dot{x}_B \\ \dot{y}_B \end{bmatrix} &= V_A^{1-7} + \begin{bmatrix} l_8 \cos(\theta_8 + \gamma) \\ -l_8 \sin(\theta_8 + \gamma) \end{bmatrix} \dot{\theta}_8 + \begin{bmatrix} l_9 \cos\theta_9 \\ l_9 \sin\theta_9 \end{bmatrix} \dot{\theta}_9.
\end{aligned}$$

3.2. DYNAMIC MODEL

3.2.1. *Non-kick Action in Single-leg-supporting Phase*

Here, the dynamic equations are studied when the biped robot has one supporting leg and there is no raising of the heel (θ_1, θ_2 constant). Applying the Lagrange dynamic model, the motion equations take the following closed form, for the case of no-kick phase:

$$\mathbf{D}(\boldsymbol{\theta})\ddot{\boldsymbol{\theta}} + \mathbf{C}(\boldsymbol{\theta}, \dot{\boldsymbol{\theta}})\dot{\boldsymbol{\theta}} + \mathbf{G}(\boldsymbol{\theta}) = \mathbf{T}_\theta, \qquad (2)$$

where $\mathbf{T}_{\theta i}$ is the generalized torque corresponding to the variable θ_i, $\mathbf{D}(\boldsymbol{\theta})$ is the positive symmetric 9×9 inertia matrix, $\mathbf{C}(\theta, \dot{\theta})$ is the 9×9 matrix (with zero diagonal terms) which includes terms from the centrifugal and Coriolis torques, and $\mathbf{G}(\boldsymbol{\theta})$ is the 9-dimensional vector which includes the gravitational torques. The form of these matrices is given in [5], and, due to space limitation, are not included here.

3.2.2. *Kick Action in Single-leg-supporting Phase*

As mentioned before, since our biped robot has a 2-link foot, here we adopt the biped locomotion mode with kick-action (only in the single leg support phase) which was firstly employed in Kenkyaku-2 [1]. A very good example of natural and dynamic biped locomotion is human walking. In fact, human walking utilizes the gravity effect very skillfully and does not depend on the ankle torque of the supporting leg so much. For example, natural stop-motion is achieved by reducing its angular momentum using the gravity effect. However, as seen from the shape of the human foot, the ankle torque of the supporting leg can decrease the walking speed but cannot increase it. Since the reduction of the speed causes

an energy loss, and according to the assumption that the biped robot has to follow a ballistic model (to keep its energy at a constant level), the ankle joint of the supporting leg is set to be free, except for the kick phase when raising of the heel exists. As a result, an additional variation of the angle θ_2 occurs, while the angle θ_1 keeps on a constant value. Using again the Lagrange dynamic model, the motion equations, during the kick phase, take a form similar to (2) (the matrices $\mathbf{D}$, $\mathbf{C}$, $\mathbf{G}$ are similar to the corresponding matrices of the previous phase, with some additional terms caused by the raising of the heel, see [5]).

In the two previous phases, introducing the transformations

$$\begin{aligned} q_1 &= \theta_1 + \theta_2 & q_5 &= \theta_5 + \theta_6 \\ q_2 &= -90^\circ + \varepsilon + \theta_2 - \theta_3 & q_6 &= \theta_6 - \theta_7 \\ q_3 &= \theta_3 - \theta_4 & q_7 &= -90^\circ + \varepsilon + \theta_8 + \theta_7 \\ q_4 &= \theta_4 - \theta_5 & q_8 &= \theta_8 + \theta_9 \end{aligned}$$

$$\boldsymbol{\tau}_i = \sum_{j=1}^{9} T_{\theta j} \frac{\partial \theta_j}{\partial q_i} \quad (i = 1, \ldots, 8),$$

where q_i is the joint angular position, and τ_i is the real driving torque exerted by each independent actuator to each joint of the biped robot (the torque at the toes of the supporting leg is zero because of the existence of one unpowered d.o.f.), one gets the following closed form of dynamic equations

$$\mathbf{D}(\mathbf{q})\ddot{\mathbf{q}} + \mathbf{C}(\mathbf{q}, \dot{\mathbf{q}})\dot{\mathbf{q}} + \mathbf{G}(\mathbf{q}) = \boldsymbol{\tau}.$$

This dynamic model will be used in the control part of the paper.

3.2.3. *Leg-support-exchange*

The walking pattern adopted in this paper implies that the leg-support-exchange is done in an instant, and therefore the double-leg-supporting phase is omitted. Then, immediately after the touchdown of the swing leg, the exchange of the supporting leg takes place. Hence, just before the collision, the biped robot is instantly on the air. As a consequence, at the time of the swing leg collision with the ground, the constraint $x_T = y_T =$ constant, which exists during the single leg supporting phase, is lost. In this case, given the fact that the motion of the biped robot is constrained on the sagittal plane, two more variables (the coordinates x_T, y_T of the supporting leg toes) are required for an exact description of the position of the biped robot. The elements of the inertial matrix $\mathbf{D}_{\mathrm{a}}$ for this case can again be found in [5].

3.2.4. *Collision of the Swing Leg with the Ground*

For a mobile robot, the collision with the environment is an ordinary affair. The collision of a robotic system with the environment may be handled as an impact

problem. There are two issues related to the impact problem. The first is how the collision changes the generalized states of the system which are externally observable. The second is how the collision brings impulsive forces to a robotic system. These forces occur internally and are not observable.

One of the effects of robot collision with the environment is the abrupt change of the joint angular velocities. Hence, a suitable mathematical model must be derived to establish the quantitative relationship between this abrupt change and the severity of the collision. Here, after the instant at which the 9-link biped robot is on the air, the touchdown of the foot of the swing-leg follows, and, as a result, the exchange of the supporting leg occurs. As mentioned in the walking pattern description (Section 2), the collision with the ground takes place in two stages. Firstly, the toes (B) of the swing leg collide with the ground and then the collision of the heel (A) follows. Thus the velocity change is given by [6]:

$$\Delta\dot{\theta} = \mathbf{D}_{\mathrm{a}}^{-1}\,{}^{B}\mathbf{J}_{\mathrm{a}}^{T}\left({}^{B}\mathbf{J}_{\mathrm{a}}\mathbf{D}_{\mathrm{a}}^{-1}\,{}^{B}\mathbf{J}_{\mathrm{a}}^{T}\right)^{-1}\Delta\dot{\mathbf{x}}_{\mathrm{B}}, \tag{3}$$

where $\mathbf{D}_{\mathrm{a}}$ is the inertia matrix of the robot model when it is instantly on the air, and ${}^{B}\mathbf{J}_{\mathrm{a}}$ is the associated Jacobian matrix. After the first collision, the velocity of the toes (B) of the swing leg vanishes. Hence

$$\underset{\text{after}}{\dot{\theta}_{B}} = \underset{\text{before}}{\dot{\theta}_{B}} + \mathbf{D}_{\mathrm{a}}^{-1}\,{}^{B}\mathbf{J}_{\mathrm{a}}^{T}\left({}^{B}\mathbf{J}_{\mathrm{a}}\mathbf{D}_{\mathrm{a}}^{-1}\,{}^{B}\mathbf{J}_{\mathrm{a}}^{T}\right)^{-1}\left(-\underset{\text{before}}{\dot{\mathbf{x}}_{B}}\right). \tag{4}$$

Then, the collision of the heel (A) of the swing leg occurs, in which case the velocity change is given by:

$$\Delta\dot{\theta} = \mathbf{D}_{\mathrm{a}}^{-1}\,{}^{A}\mathbf{J}_{\mathrm{a}}^{T}\left({}^{A}\mathbf{J}_{\mathrm{a}}\mathbf{D}_{\mathrm{a}}^{-1}\,{}^{A}\mathbf{J}_{\mathrm{a}}^{T}\right)^{-1}\Delta\dot{\mathbf{x}}_{A}, \tag{5}$$

where

$${}^{A}\mathbf{J}_{\mathrm{a}} = \begin{bmatrix} \dfrac{\partial \mathbf{x}_A}{\partial\theta_1} & \dfrac{\partial \mathbf{x}_A}{\partial\theta_2} & \cdots & \dfrac{\partial \mathbf{x}_A}{\partial\theta_9} & \dfrac{\partial \mathbf{x}_A}{\partial \mathbf{x}_T} & \dfrac{\partial \mathbf{x}_A}{\partial \mathbf{y}_T} \\ \dfrac{\partial \mathbf{y}_A}{\partial\theta_1} & \dfrac{\partial \mathbf{y}_A}{\partial\theta_2} & \cdots & \dfrac{\partial \mathbf{y}_A}{\partial\theta_9} & \dfrac{\partial \mathbf{y}_A}{\partial \mathbf{x}_T} & \dfrac{\partial \mathbf{y}_A}{\partial \mathbf{y}_T} \end{bmatrix}.$$

Similar to the first case, after the second collision, the velocity of the heel (A) goes to zero. Thus

$$\underset{\text{after}}{\dot{\theta}_{A}} = \underset{\text{before}}{\dot{\theta}_{A}} + \mathbf{D}_{\mathrm{a}}^{-1}\,{}^{A}\mathbf{J}_{\mathrm{a}}^{T}\left({}^{A}\mathbf{J}_{\mathrm{a}}\mathbf{D}_{\mathrm{a}}^{-1}\,{}^{A}\mathbf{J}_{\mathrm{a}}^{T}\right)^{-1}\left(-\underset{\text{before}}{\dot{\mathbf{x}}_{A}}\right), \tag{6}$$

where

$$\underset{\text{before}}{\dot{\theta}_{A}} = \underset{\text{after}}{\dot{\theta}_{B}},$$

which is computed from the first collision.

From this relation one can compute the angular velocities of the joints after the collision and the exchange of the supporting leg. In practice each robotic

joint is equipped with an angular velocity sensor. An instantaneous change of the sensor output indicates the occurrence of a collision. To recover the motion from a collision, a special effort should then be made by the controller.

4. Sliding-mode Robust Control of the 9-link Biped Robot

The locomotion activity, and gait in particular, is a highly automated motion. When a man is walking in a steady regime or in an environment imposing small disturbances, the central nervous system is not involved. However, when large disturbances occur, the system actions are directed only to the preservation of the system overall stability, i.e., towards preventing the system from falling down. This requirement is of primary importance in biped locomotion.

Usually, the control of biped and multi-legged robots has a hierarchical structure, which most often is vertical, so that each control level deals with some wider aspects of the overall system behaviour than the next lower level. A higher control level always refers to the lower ones, and controls those system parameters that vary more slowly. A higher control level communicates with a lower level, giving to it instructions, and receiving from it relevant information required for the decision-making process. After obtaining the information from a lower level, each hierarchical level makes decisions taking into account general instructions obtained from a higher level, and forwards them to the lower level for execution.

In general, four hierarchical levels are used in robot control, namely:

1. The *highest (organizational) level*, which recognizes the obstacles in the operating space and the conditions under which a task is carried out, and decides how the required task has to be accomplished.
2. The *strategic level*, which divides the imposed operation into elementary movements.
3. The *tactical level*, which performs the distribution of an elementary movement to the motion of each d.o.f. of the robot.
4. The *execution level*, which executes the desired motion of each d.o.f. via suitable actuators.

The complexity of the control structure for locomotion robots depends primarily on whether the robot walks on a terrain of known or unknown profile. The walking on a terrain of unknown profile requires all four hierarchical control levels, also employing techniques of artificial intelligence. If the walk is performed on a terrain of known profile, then only the two lowest control levels are required. The trajectories of each link can be defined off-line, as well as the corresponding torques and controls of each actuator. All these data may be stored at the robot controller and used when the walk is performed. This is a problem which is solved at the tactical level. Then, the task imposed at the execution level is how to ensure the achievement of the precalculated trajectories if a certain perturbation occurs. This problem reduces to that of eliminating the deviation of

the actual system state from the precalculated one, and this is the only part of the control task which should be solved in real time.

To face the important problem of stability, the control design must be performed in two stages. At the first stage, called the *stage of nominal regimes*, the control has to be designed so as to ensure the system's motion along the exact nominal trajectories calculated in advance in the absence of any disturbance. It has to satisfy the conditions of both the desired gait type and overall system equilibrium. The nominal trajectories ensure that the system is in equilibrium under ideal conditions, i.e., when the model of the system is perfect, the trajectories are perfectly realized, and no perturbations are acting upon the system. Since these conditions are never fulfilled, additional control is necessary to ensure the tracking of these nominal trajectories and preserve the system equilibrium in the presence of disturbances. Hence at the second stage, called the *stage of perturbed regimes*, only the deviation of the actual state vector from its nominal value is considered, and additional control is applied to force the system state to its nominal. To this end, various approximate methods have been proposed. The most frequently used technique in the control of biped robots is the simple decentralized controller, which assumes that each joint is controlled independently from the rest of the system.

However, a decentralized controller cannot stabilize the entire system because of the strong dynamic coupling between the joints, and the necessity to indirectly control unpowered d.o.f. and to preserve the system equilibrium in the perturbed regimes. Therefore additional feedback loops have to be designed and applied. A method that has been proposed is the application of *global control by force feedback* and by *on-line computation of the dynamic coupling* between the joints. By measuring the moments at the joints one gets direct information on the coupling between them. Thus, one may easily establish the global control which can compensate for the effects of joint coupling. Similarly, by measuring the forces between the sole of the supporting leg and the ground, one may establish the global control which would maintain the system equilibrium.

A measure of the system overall deviation from nominal trajectories, which is usually adopted, is the deviation of the *zero moment point* (ZMP) from its nominal position. The actual position of the ZMP can be computed from the measured values of the vertical reaction forces acting from the ground upon the supporting feet. By using these reaction forces, an additional feedback can be introduced that enables the system to maintain itself in the equilibrium state, i.e., to keep the ZMP position within a limited area. Therefore, the control which aims to ensure the stability of a biped robot must take into account the dynamics of the system.

In this paper we follow this path and consider the possibility of implementing global control by on-line computation of the dynamic forces. This means that: (i) the control computer has to compute the dynamic moments about the biped joints at every 1–2 ms in order to achieve a sampling rate compatible with the system

dynamics (in particular, if the algorithms are programmed in *assembly*, the computation time is of the order of 3–4 ms, but using suitable fast inverse dynamics algorithms, or parallelizing the computations, this figure can go down to less than 1–2 ms – another improvement can be obtained if all the trigonometric functions involved are prestored and called from a ROM memory); (ii) nonlinear control may be necessary for achieving the desired peformance, since the tasks of a biped robot involve large range and/or high speed motions. Therefore, the computed torque control law has been proposed, which is a special type of feedback linearization for rigid robots. This nonlinear feedback technique transforms the highly coupled and nonlinear robot dynamics into equivalent, decoupled linear systems (one for each d.o.f.) and then the well known and powerfull linear design techniques can be used to complete the control design.

This approach is based on the assumption that an accurate model of the biped robot is known, a condition that is never fulfilled because of the existence: (i) of structured uncertainties which correspond to inaccuracies in the model parameters (e.g., imprecision on the mass properties or the loads or the robot geometry, and inaccuracies on the torque constants of the actuators) or to additive disturbances (e.g., Coulomb friction, and stiction), and (ii) of unstructured uncertainties (unmodeled dynamics), which reflect the errors on the system order (e.g., structural resonant modes, neglected time delays, and finite sampling rate). Actually, the problem is that we only have an estimation $\widehat{\mathbf{D}}(\mathbf{q})$, $\widehat{\mathbf{C}}(\mathbf{q}, \dot{\mathbf{q}})$ of the inertia matrix $\mathbf{D}(\mathbf{q})$ and the matrix $\mathbf{C}(\mathbf{q}, \dot{\mathbf{q}})$ which represents the centrifugal, Coriolis, gravitational and friction torques. Hence, the closed-loop system takes the form:

$$\ddot{\mathbf{q}} = (\mathbf{D}^{-1}\widehat{\mathbf{D}})\boldsymbol{\tau} + \mathbf{D}^{-1}(\widehat{\mathbf{C}} - \mathbf{C}) \tag{7}$$

and the objective is to design a control input $\boldsymbol{\tau}$ (probably nonlinear) which minimizes the sensitivity of the system performance under the presence of dynamic model uncertainty.

In this paper, it is assumed that: (i) the dynamic model of the 9-link biped robot is not exactly known, and (ii) the estimation error of unknown (and probably time-varying) parameters is bounded by some known function. Hence, we employ a sliding-mode controller which provides a successful way for maintaining stability and consistent performance in the presence of modeling imprecisions, and at the same time is able to quantify the resulting modeling/performance trade offs (for example, the effect of discarding any particular term of the dynamic model on the tracking performance).

The dynamic model of the biped robot with n d.o.f. has the general form (see Equation (2)):

$$\mathbf{D}(\mathbf{q})\ddot{\mathbf{q}} + \mathbf{C}(\mathbf{q}, \dot{\mathbf{q}})\dot{\mathbf{q}} + \mathbf{G}(\mathbf{q}) = \boldsymbol{\tau}, \tag{8}$$

where $\mathbf{D}(\mathbf{q})$ is the $n \times n$ inertia matrix (which is symmetric and positive definite), $\mathbf{C}(\mathbf{q}, \dot{\mathbf{q}})\dot{\mathbf{q}}$ is an n-vector of centripetal and Coriolis torques ($\mathbf{C}(\mathbf{q}, \dot{\mathbf{q}})$ is a $n \times n$ matrix), and $\mathbf{G}(\mathbf{q})$ is the n-vector of gravitational torques.

By looking at the physics of the biped robot, one verifies that the matrix $(\dot{\mathbf{D}} - 2\mathbf{C})$ is skew-symmetric (a very important property of robot dynamics). Furthemore one notes that, since $\mathbf{D}$ and therefore $\dot{\mathbf{D}}$, are symmetric matrices, the skew-symmetricity of the matrix $(\dot{\mathbf{D}} - 2\mathbf{C})$ can also be written as:

$$\dot{\mathbf{D}} = \mathbf{C} + \mathbf{C}^T. \tag{9}$$

Now, define a time-varying surface $S(t)$ in the state-space $\Re^n$ by the vector equation $\mathbf{s}(\mathbf{q}; \mathbf{t}) = 0$, with

$$s_i = \Big(\frac{\mathrm{d}}{\mathrm{d}t} + \lambda_i\Big)\tilde{q}_i, \tag{10}$$

where $\tilde{q}_i = q_i - q_{d_i}$ is the tracking error at the ith joint, and λ_i is a strictly positive constant which symbolizes the control bandwidth. Hence, the vector $\mathbf{s}$ is defined as

$$\mathbf{s} = \dot{\tilde{\mathbf{q}}} + \mathbf{\Lambda}\tilde{\mathbf{q}}, \tag{11}$$

where $\mathbf{\Lambda}$ is a symmetric positive definite matrix, or more generally a matrix such that $\mathbf{\Lambda}$ is Hurwitz.

Furthemore, $\mathbf{s}$ can be interpreted as a 'velocity error' term

$$\mathbf{s} = \dot{\mathbf{q}} - \dot{\mathbf{q}}_\mathbf{r}, \tag{12}$$

where

$$\dot{\mathbf{q}}_\mathbf{r} = \dot{\mathbf{q}}_\mathbf{d} - \mathbf{\Lambda}\tilde{\mathbf{q}}. \tag{13}$$

The 'reference velocity' vector $\dot{\mathbf{q}}_\mathbf{r}$ is formed by shifting the desired velocities $\dot{\mathbf{q}}_\mathbf{d}$ according to the position error $\tilde{\mathbf{q}}$. It simply provides a notational representation that allows the translation of energy-related properties (expressed in terms of the actual joint velocity vector $\dot{\mathbf{q}}$) into trajectory control properties (expressed in terms of the virtual velocity error vector $\mathbf{s}$).

The vector $\mathbf{s}$ conveys information about the boundedness and convergence of $\mathbf{q}$ and $\dot{\mathbf{q}}$, since the definition Equation (11) of $\mathbf{s}$ can also be viewed as a stable first-order differential equation in $\tilde{\mathbf{q}}$, with $\mathbf{s}$ as an input. Hence, *given initial conditions* $\mathbf{q}_\mathbf{d}(t = 0) = \mathbf{q}(t = 0)$, *the problem of tracking* $\mathbf{q}(t) \equiv \mathbf{q}_\mathbf{d}(t)$ *is equivalent to that of remaining on the surface* $S(t)$ *for all* $t > 0$. Indeed, $\mathbf{s} \equiv 0$ represents a set of linear differential equations whose unique solution is $\tilde{\mathbf{q}} \equiv 0$ (given the above initial condition).

The simplified objective of keeping the scalar s_i at zero can now be achieved by choosing the control law such that outside of $S(t)$ the following condition holds:

$$\frac{1}{2}\frac{\mathrm{d}}{\mathrm{d}t}s_i^2 \leqslant -\eta_i|s_i|, \tag{14}$$

where η_i is a strictly possitive constant. Essentialy, (14) states that the squared 'distance' to the surface, as measured by $\mathbf{s}^2$, decreases along all system trajectories. Thus, it constraints the trajectories to point towards the surface $S(t)$.

The basic idea behind Equations (10) and (14) is to pick up a well behaved function of the tracking error $\mathbf{s}$, according to (10), and then select the feedback control law such that $\mathbf{s}^2$ remains a Lyapunov-like function of the closed loop system, despite the presence of model imprecisions and disturbances. Hence, if

$$V(s,t) = (1/2)\mathbf{s}\mathbf{s}^T$$

then based on Lyapunov theory for non-autonomous systems and by virtue of the properties:

(i) $V(\mathbf{s},t)$ is a positive definite, scalar function with continuous partial derivatives;
(ii) $V(\mathbf{s},t) \to \infty$ as $\|\mathbf{s}\| \to \infty$;
(iii) $\dot{V}(\mathbf{s},t) \leqslant -\eta|\mathbf{s}| \Rightarrow \dot{V}(\mathbf{s},t) < 0$ (for $\mathbf{s} \neq 0$)

we come to the conclusion that $\mathbf{s} \equiv 0$ is a globally asymptotically stable equilibrium point. Therefore, the sliding surface $S(t)$ becomes an invariant set. In particular, once on the surface, the system trajectories remain on the surface. Furthemore, these properties imply that some disturbances or dynamic uncertainties can be tolerated while still keeping the surface an invariant set.

We are now ready to address the robust trajectory control problem. Let us define:

$$V(t) = (1/2)[\mathbf{s}^T\mathbf{D}\mathbf{s}]. \tag{15}$$

Differentiating $V(t)$ gives:

$$\dot{V}(t) = \mathbf{s}^T(\mathbf{D}\ddot{\mathbf{q}} - \mathbf{D}\ddot{\mathbf{q}}_\mathbf{r}) + (1/2)\mathbf{s}^T\dot{\mathbf{D}}\mathbf{s}.$$

Therefore, substituting $\mathbf{D}\ddot{\mathbf{q}}$ from the system dynamics,

$$\mathbf{D}\ddot{\mathbf{q}} = \boldsymbol{\tau} - \mathbf{C}\dot{\mathbf{q}} - \mathbf{G} = \boldsymbol{\tau} - \mathbf{C}(\mathbf{s} + \dot{\mathbf{q}}_\mathbf{r}) - \mathbf{G}$$

yields

$$\dot{V}(t) = \mathbf{s}^T(\boldsymbol{\tau} - \mathbf{D}\ddot{\mathbf{q}}_\mathbf{r} - \mathbf{C}\dot{\mathbf{q}}_\mathbf{r} - \mathbf{G}),$$

where the skew-symmetry of $(\dot{\mathbf{D}} - 2\mathbf{C})$ has been used to eliminate the term $(1/2)\mathbf{s}^T\dot{\mathbf{D}}\mathbf{s}$.

Now, define the control input to be of the form

$$\boldsymbol{\tau} = \hat{\boldsymbol{\tau}} - \mathbf{K}\mathrm{sgn}(\mathbf{s}), \tag{16}$$

where $\mathbf{K}\mathrm{sgn}(\mathbf{s})$ is defined as the vector with components $K_i\mathrm{sgn}(s_i)$, and $\hat{\boldsymbol{\tau}}$ is the control input vector which would make $\dot{V}$ equal to zero if the dynamics were exactly known ($\widehat{\mathbf{D}} = \mathbf{D},\ \widehat{\mathbf{C}} = \mathbf{C},\ \widehat{\mathbf{G}} = \mathbf{G}$):

$$\hat{\boldsymbol{\tau}} = \widehat{\mathbf{D}}\ddot{\mathbf{q}}_\mathbf{r} + \widehat{\mathbf{C}}\dot{\mathbf{q}}_\mathbf{r} + \widehat{\mathbf{G}}. \tag{17}$$

We then have

$$\dot{V} = \mathbf{s}^T \left[\widetilde{\mathbf{D}}(\mathbf{q})\ddot{\mathbf{q}}_\mathbf{r} + \widetilde{\mathbf{C}}(\mathbf{q}, \dot{\mathbf{q}})\dot{\mathbf{q}}_\mathbf{r} + \widetilde{\mathbf{G}}(\mathbf{q})\right] - \sum_i^n K_i |s_i|.$$

As mentioned before, because of the parametric uncertainty, the only a priori knowledge we have available are the bounds of the estimation errors:

$$\widetilde{\mathbf{D}} = \widehat{\mathbf{D}} - \mathbf{D}, \qquad \widetilde{\mathbf{C}} = \widehat{\mathbf{C}} - \mathbf{C}, \quad \text{and} \quad \widetilde{\mathbf{G}} = \widehat{\mathbf{G}} - \mathbf{G}.$$

Now, we can easily see that choosing the components K_i of the vector $\mathbf{K}$ such that

$$K_i \geqslant \left| \left[\widetilde{\mathbf{D}}(\mathbf{q})\ddot{\mathbf{q}}_\mathbf{r} + \widetilde{\mathbf{C}}(\mathbf{q}, \dot{\mathbf{q}})\dot{\mathbf{q}}_\mathbf{r} + \widetilde{\mathbf{G}}(\mathbf{q})\right]_i \right| + \eta_i, \tag{18}$$

where the constants η_i are strictly positive, allows one to satisfy the sliding condition

$$\dot{V} \leqslant -\sum_{i=1}^n \eta_i |s_i|. \tag{19}$$

The above sliding condition guarantees that the surface $\mathbf{s} = 0$ is reached in a finite time, and that, once on the surface, the trajectories remain on the surface and, therefore, tend to $\mathbf{q_d}(t)$ exponentially.

However, as can be seen from (16), in order to account for the presence of modeling imprecision, the control law has to be discontinuous across $S(t)$. Since the implementation of the associated control switchings is necessarily imperfect, this leads to chattering which is undesirable in practice, since it involves high control activity and may excite high frequency dynamics neglected in the course of modeling (such as unmodeled dynamics modes, neglected time delays, and so on). Thus, in a further step, the discontinuous control law $\boldsymbol{\tau}$ is suitably smoothed, in order to achieve robustness to high frequency unmodeled dynamics.

This can be done by smoothing out the control discontinuity in a thin boundary layer $B(t)$ neighboring the switching surface:

$$B(t) = \{\mathbf{q},\ |s_i(\mathbf{q}, t)| \leqslant \Phi_i\}, \quad \boldsymbol{\Phi} > 0,$$

where $\boldsymbol{\Phi}$ is the boundary layer thickness. In other words, outside $B(t)$ we choose the control law as before, which guarantees that the boundary layer is attractive and hence invariant (all trajectories starting inside $B(t = 0)$ remain inside $B(t)$ for all $t \geqslant 0$), and then we interpolate $\boldsymbol{\tau}$ inside $B(t)$, replacing the term $\text{sgn}(s_i)$ by s_i/Φ_i in the expression of $\boldsymbol{\tau}$.

Thus, instead of simply requiring (14) to be satisfied outside the boundary layer, we now require that

$$|\mathbf{s}| \geqslant \mathbf{\Phi} \Rightarrow \frac{1}{2}\frac{\mathrm{d}}{\mathrm{d}t}[\mathbf{s}^T\mathbf{D}\mathbf{s}] \leqslant (\mathbf{\Phi} - \boldsymbol{\eta})|\mathbf{s}|. \tag{20}$$

In order to satisfy (20), the quantity $-\Phi_i$ is added to the control discontinuity gain K_i. Accordingly, the control law $\boldsymbol{\tau}$ becomes:

$$\boldsymbol{\tau} = \hat{\boldsymbol{\tau}} - \overline{\mathbf{K}}\,\mathrm{sat}\Big(\frac{\mathbf{s}}{\mathbf{\Phi}}\Big), \tag{21}$$

where

$$\overline{\mathbf{K}} = \mathbf{K} - \mathbf{\Phi}. \tag{22}$$

The effect of control interpolation in a boundary layer can be discussed further, and help to select the design parameters λ_i and Φ_i. In fact, the ranges Φ_i of the interpolation can be chosen so that the maximum value of each $\overline{K}_i/\Phi_i$ is approximately equal to the control badwidth λ_i. This condition could give an approximate trade-off between control bandwidth (which represents the robustness to unmodeled dynamics), tracking precision, and parametric uncertainty (which is represented by $\overline{\mathbf{K}}$).

For our 9-link biped robot, we have assumed that although the accuracy of the estimation of the robot dynamic parameters is not known, we have available the limits of the unknown parameter uncertainty (i.e., the bound of our estimation error). For the experiments we have assumed a maximum uncertainty of 45% on the mass properties (mass m_i, rotational inertia I_i) of the biped robot, and 10%, and 20% on the link length l_i and on the radius d_i of the c.o.g. from the lower joint, respectively, i.e.,

$$|m_i - \hat{m}_i| \leqslant 0.45\hat{m}_i, \qquad |I_i - \hat{I}_i| \leqslant 0.45\hat{I}_i, \qquad |l_i - \hat{l}_i| \leqslant 0.1\hat{l}_i,$$
$$|d_i - \hat{d}_i| \leqslant 0.2\hat{d}_i.$$

Based on the estimates $\hat{m}_i$, $\hat{I}_i$, $\hat{l}_i$ and $\hat{d}_i$ of the parameters, and on the limits em, eI, el and ed of the uncertainty, one can compute the bounds of the modeling errors, as:

$$\begin{aligned}\widetilde{D}_{11} \;\leqslant\; & [(1+eI)\hat{I}_1 - \hat{I}_1] + [(1+em)\hat{m}_1(1+ed)^2\hat{d}_1 - \hat{m}_1\hat{d}_1^2] \\ & + [(1+em)(\hat{m}_3 + \cdots + \hat{m}_9)(1+el)^2\hat{l}_1^2 - (\hat{m}_3 + \cdots + \hat{m}_9)\hat{l}_1^2] \\ =\; & eI\hat{I}_1 + \hat{m}_1\hat{d}_1^2[(1+em)(1+ed)^2 - l] \\ & + (\hat{m}_3 + \cdots + \hat{m}_9)\hat{l}_1^2[(1+em)(1+el)^2 - l].\end{aligned}$$

The bounds for the other terms can be computed in the same way.

A first key question is to determine how large $\mathbf{\Lambda}$ can be chosen. Although the tuning of this single scalar may in practice be done experimentally, considerable insight on the overall design can be obtained by explicitly analyzing

the various factors limiting λ_i. In mechanical systems, for instance, given clean measurements, λ_i is typically limited by the following three factors: (i) structural resonant modes, (ii) neglected time delays, (iii) sampling rate. Since in this problem we have no a priori information on the first two constraining factors, the only limit results from the last factor. Hence, by choosing a value of 0.5 kHz ($T = 2$ ms) for sampling rate, we achieve a maximum desired control bandwidth of about 100 rad/s, since $\lambda \geqslant (1/5)\nu_{\text{sampling}}$ [8]. This is a simple limit for λ_i, since in our case the ideal values have been computed through the trial and error technique in the simulations, and have also been justified by Lyapunov analysis.

Given initial conditions outside the boundary layer, and in order to achieve fast tracking of the trajectories inside this region, one must choose large values for η_i (which, formally, reflects the time to reach the boundary layer starting from the outside), since the time needed for the boundary layer to be reached by the trajectories is inversely proportional to η_i. At the same time, η_i has to be chosen small enough, compared to the average value of $\overline{\mathbf{K}}$, in order to fully exploit the available knowledge on the structure of parametric uncertainty.

Finally, the bound Φ_i of the boundary layer is selected to have small values, in order for the tracking error $\tilde{q}_i$ and the velocity error $\dot{\tilde{q}}_i$, for each joint, to be limited in small values. However, at the same time the value of Φ_i should be large enough to avoid the chattering which appears due to the discontinuous control law outside of the boundary layer. The above choice for the value Φ_i has to do with the fact that when the control discontinuity is smoothed in a thin boundary layer neighboring the switching surface, the asymptotic stability is lost, and the only things that can be achieved are: (i) a tracking error limited inside a region which is proportional to the bound Φ_i and inversely proportional to the control bandwidth λ_i, and (ii) a velocity error limited in a region which is proportional to the bound Φ_i (obviously, both errors are also dependent on the initial conditions).

5. Simulation Experimental Results

The 9-link biped robot, initially at upright posture, is commanded a desired trajectory similar to that synthesized by the reference signals adopted for the walking pattern generation (Figure 2). The corresponding angular positions and position errors, during the first two steps (in a 3.5-s interval), are shown in Figures 6 and 7, respectively. These diagrams show clearly the very good tracking of the desired reference signals, achieved despite the presence of the large uncertainty, which is also obvious from the fact that the average tracking error for the first and second steps is 0.017 rads and 0.062 rads, respectively. Figure 8 depicts the variation of the driving torques of the biped in the same interval from which one can observe: (i) the increased values of these torques required for facing the

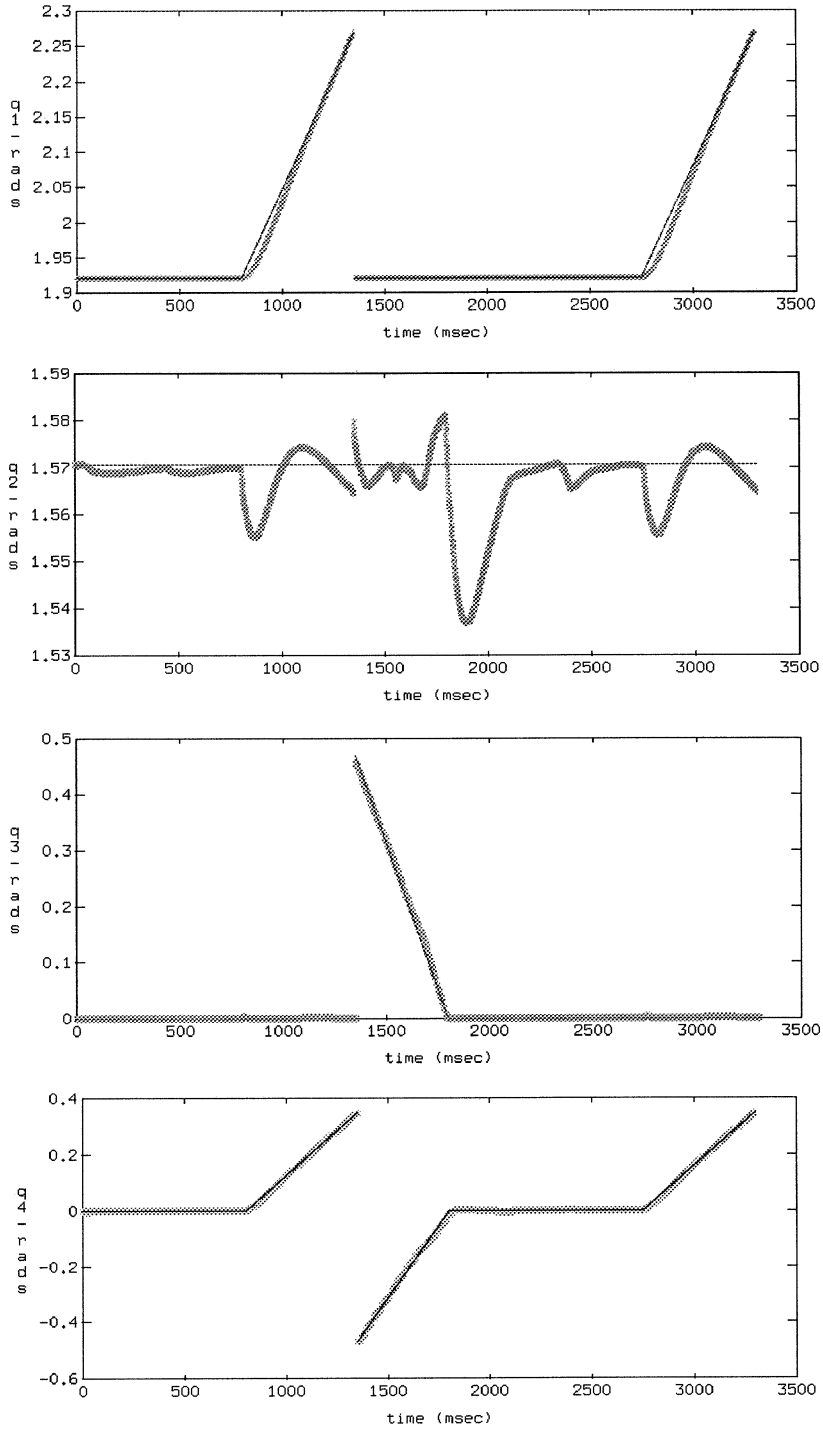

Figure 6. Angle displacements and reference signals of the 9-link, human-sized biped joints.

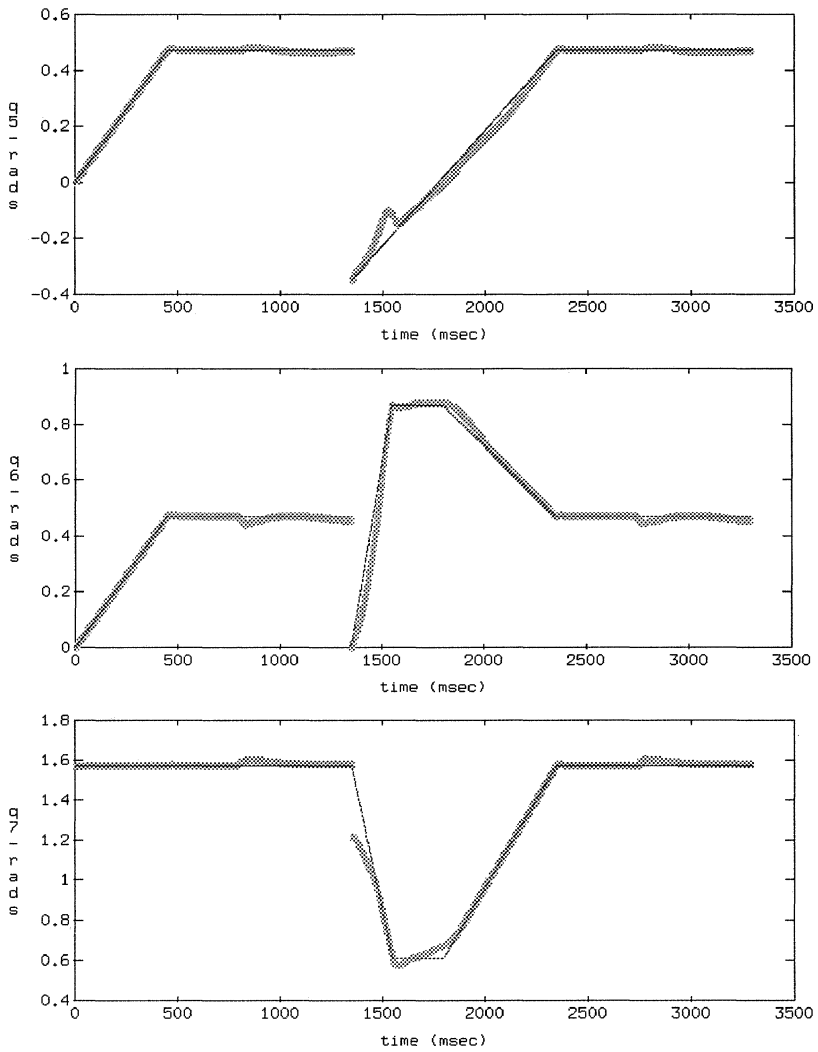

Figure 6. Continued.

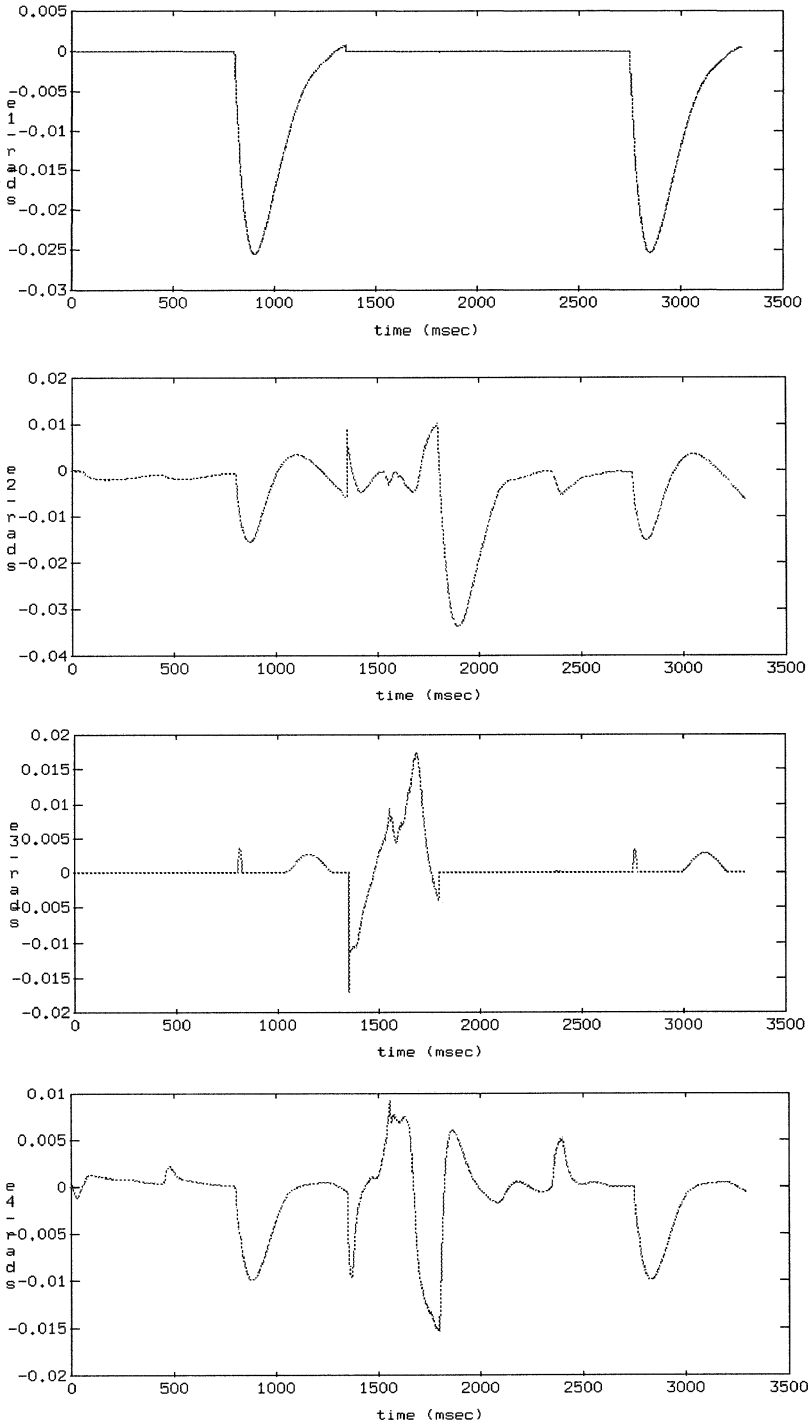

Figure 7. Angle tracking errors of the 9-link, human-sized biped joints.

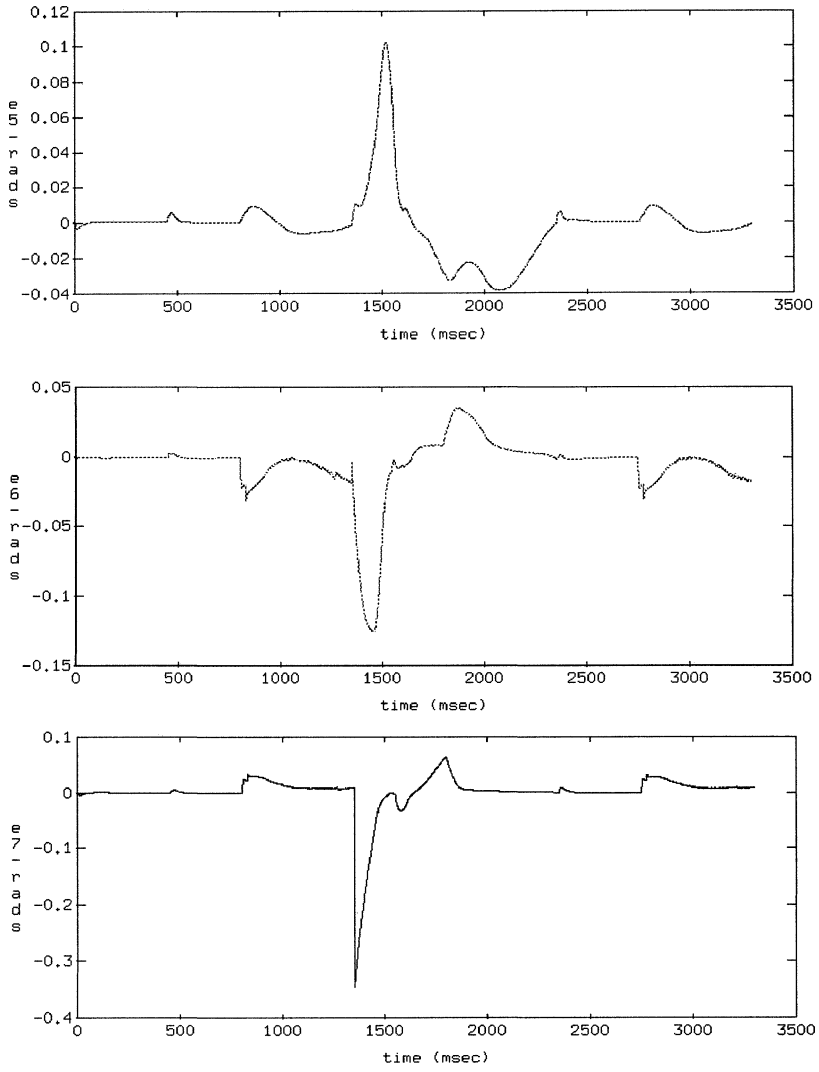

Figure 7. Continued.

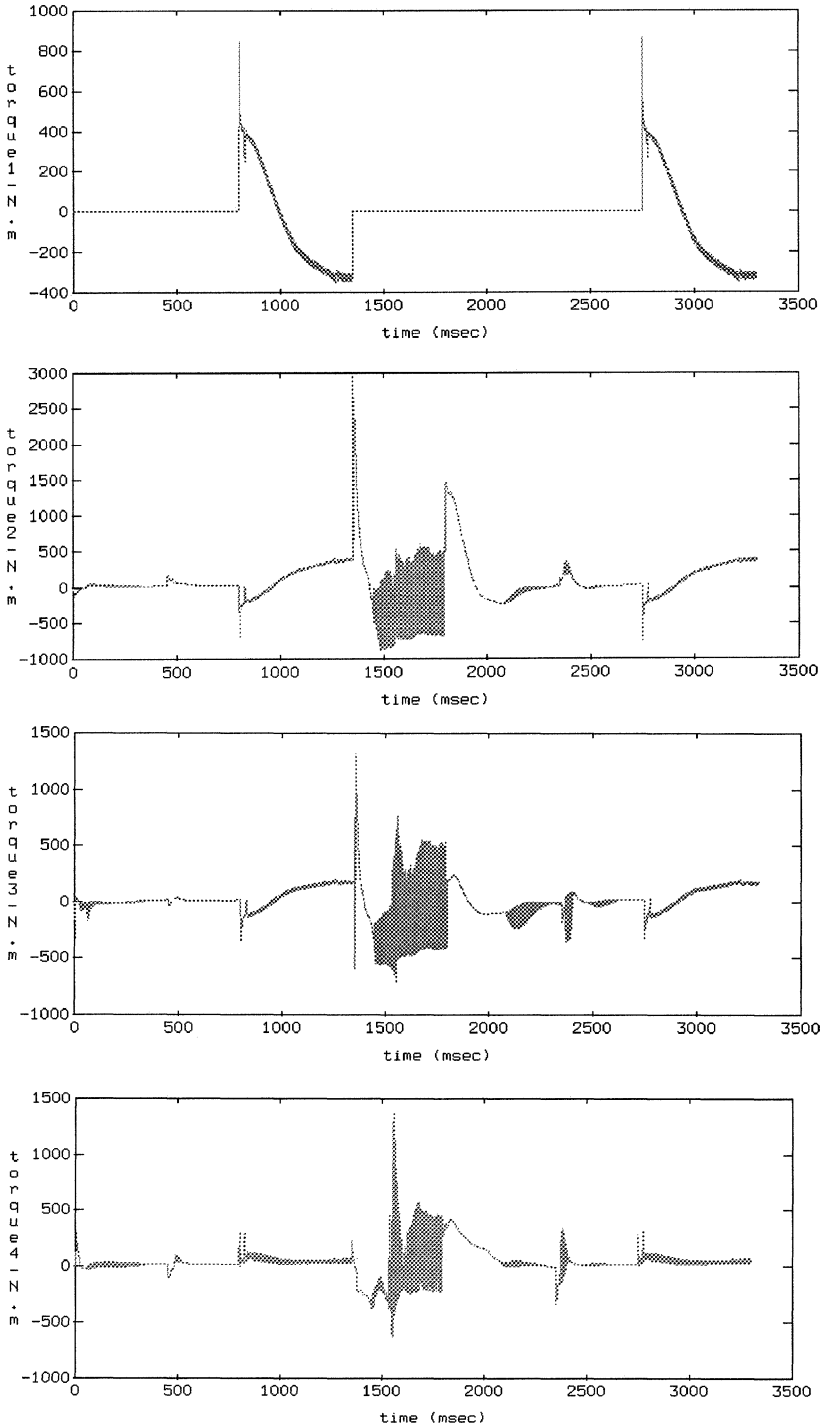

Figure 8. Driving torques of the 9-link, human-sized biped joints.

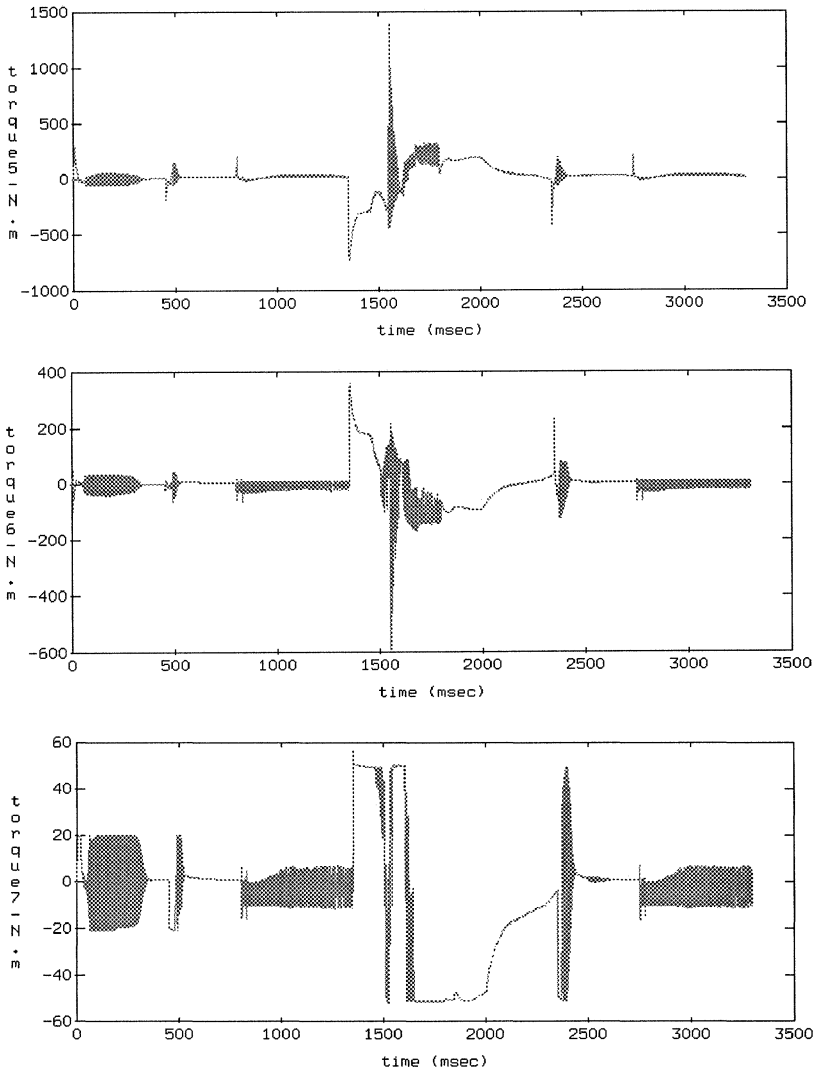

Figure 8. Continued.

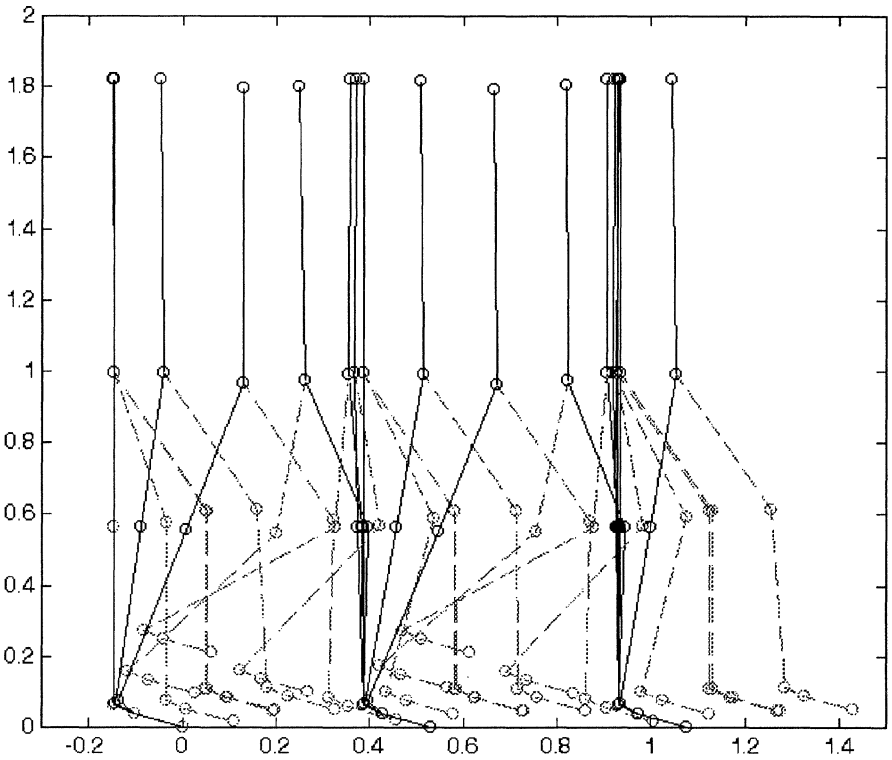

Figure 9. Locomotion mode of 9-link biped (stick diagram).

existing parametric uncertainty, and (ii) the chattering of the sliding-mode control outside the boundary layer (occurring at the beginning of each phase). Finally, the walking mode of a 9-link human-sized biped on the horizontal surface in a 5-s interval has the form of Figure 9, where one can easily see that this walking mode satisfies all necessary properties that have been adopted in Section 2 in order to utilize the gravity effect skillfully.

The present robust control technique has also been tested in the case where the actual parameter inaccuracy on the mass properties of the biped robot is larger than the maximum uncertainty of 45% which was initially assumed during the design of the sliding mode controller. The corresponding diagrams for the case where the actual parameter inaccuracy is 200% are shown in Figure 10. One can see that again a very good robustness to large parameter inaccuracies is achieved contrary to any initial expectations.

The results presented (as well as others not included here due to limited space) have fully verified the theoretically expected performance equivalence of the present sliding-mode control scheme with other robust-adaptive control techniques, especially for situations where there exist large parametric uncertainty (see, e.g., [9]).

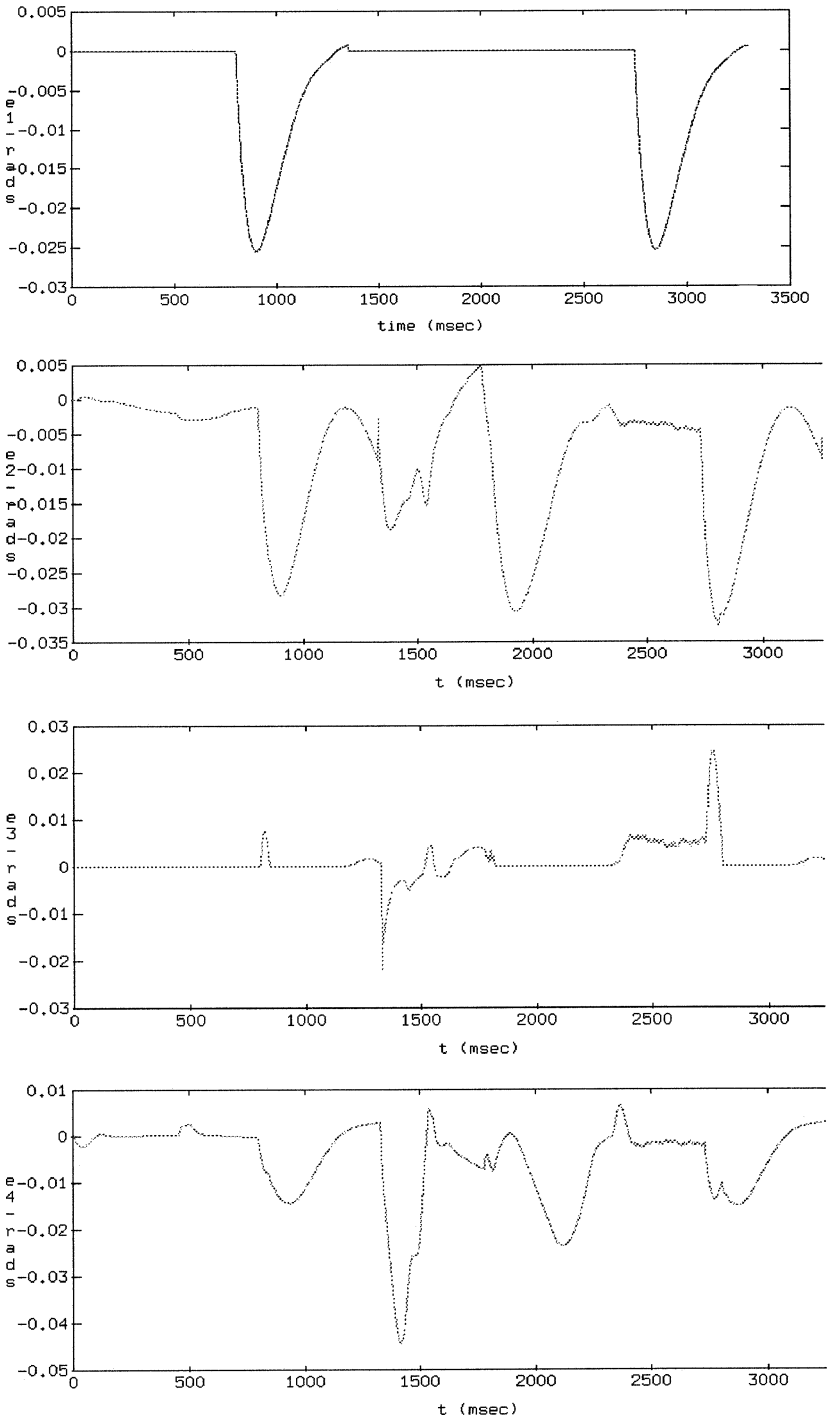

Figure 10. Angle tracking errors for the case where the actual parameter inaccuracy is 200%.

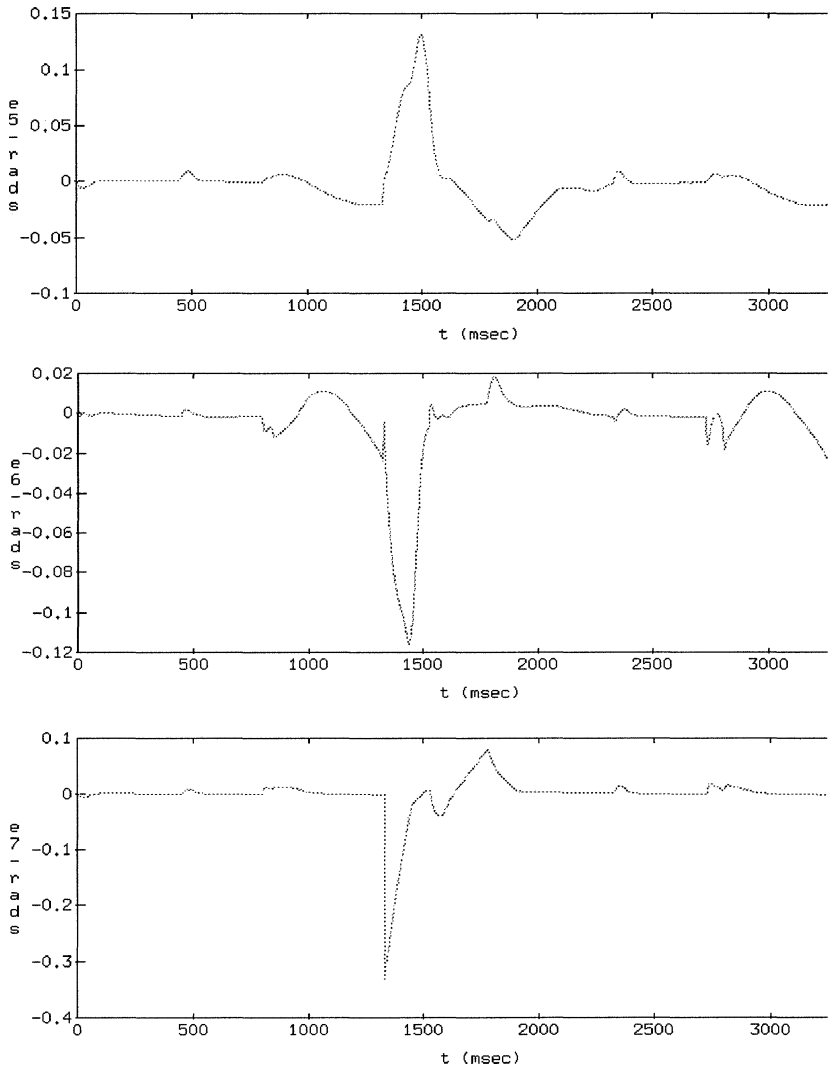

Figure 10. Continued.

6. Concluding Remarks

In this paper the effectiveness of sliding-mode robust control applied to the walking of a 9-link (8 d.o.f.) biped robot was investigated. The biped robot was assumed to involve large parametric uncertainty, while its locomotion was constrained to be on the sagittal plane. The eight degrees of freedom correspond to two hip, two knee, two ankle, and two metatarsal (foot) joints.

The sliding-mode controller ensures that the trajectories point towards the sliding surface $S(t)$ (which is actually an invariant set) and reach it starting from any initial condition in a finite time. The exact form of the control law involves

the sgn$(\cdot)$ switching function which leads to undesired 'control signal chattering'. This chattering is considerably reduced through smoothening obtained by using the saturation function in place of the signum function.

The performance of the controller was extensively tested through simulation using bipeds of several sizes, and uncertainties of several levels. In all cases (including the case of 200% parametric inaccuracy) the controller showed very good robustness and the biped was able to walk safely and accurately. Therefore, one can conclude from these experiments that sliding-mode control is a good potential scheme for application in practice.

References

1. Yamada, M., Furusho, J., and Sano, A.: Dynamic control of walking robot with kick-action, in: *Proc. 1985 Int. Conf. on Advanced Robotics (ICAR '85)*, Tokyo, 1985, pp. 405–412.
2. Tzafestas, S. G., Raibert, M., and Tzafestas, C. S.: Robust sliding-mode control applied to a 5-link biped robot, *J. of Intelligent and Robotic Systems* **15** (1996), 67–133.
3. Mochon, S.: A mathematical model of human walking, in: *Lectures on Mathematics in Life Sciences*, Vol. 14, Amer. Math. Soc., New York, 1981.
4. Hemami, H., Zheng, Y. F., and Hines, M.: Initiation of walk and tiptoe of planar nine-link biped, *Math. Biosciences* **61** (1982), 163–189.
5. Tzafestas, S. G., Krikochoritis, T. E., and Tzafestas, C. S.: Robust adaptive gait control of a 9-link biped robot, Tech. Report, IRAL/ECE Dept., NTUA, Greece, Dec. 1996.
6. Zheng, Y. F. and Hemami, H.: Impact effects of biped contact with the environment, *IEEE Trans. Systems Man Cybernet.* **14**(3) (1984), 437–443.
7. Vukobratovic, M., Borovac, B., Surla, D., and Stokic, D.: *Scientific Fundamentals of Robotics 7-Biped Locomotion (Dynamics, Stability, Control and Application)*, Springer, Berlin, 1990.
8. Slotine, J. J. and Li, W.: *Applied Nonlinear Control*, Prentice-Hall, 1992.
9. Tzafestas, S. G., Krikochoritis, T. E., and Tzafestas, C. S.: A robust-adaptive locomotion controller for 9-link bipeds with rapidly varying unknown parameters, in: *5th IEEE Mediterranean Conf. on Control and Systems*, Cyprus, July 1997.